SMAP Enhanced-Resolution Scatterometer and Synthetic Aperture Radar Image Products

Julie Z. Miller, David G. Long, Mary J. Brodzik, and Molly A. Hardman

***Abstract*—The MEaSUREs Calibrated Enhanced-Resolution Passive Microwave Daily *EASE-Grid 2.0* Brightness Temperature (CETB) Earth Science Data Record and the SMAP Twice-Daily rSIR-Enhanced *EASE-Grid 2.0* Brightness Temperature (SETB) Data Set provide an extensive multi-instrument, multi-decadal, time series of global enhanced-resolution microwave radiometer image products. The Earth-based CETB and SETB archives are generated using swath-based multi-frequency microwave brightness temperature (T^B) observations collected by the Nimbus-7 Scanning Multichannel Microwave Radiometer (SMMR), the Special Sensor Microwave/Imager (SSM/I) and Special Sensor Microwave Imager/Sounder (SSMIS) series, the Advanced Microwave Scanning Radiometer–Earth Observing System (AMSR-E), and the Soil Moisture Active Passive (SMAP) microwave radiometer. In this paper, we describe new global SMAP enhanced-resolution scatterometer and synthetic aperture radar (SAR) image products that augment the CETB and SETB archives. Earth-based, morning and evening images are generated using swath-based L-band (1.26 GHz) radar backscatter (σ^o) observations and previous developed image reconstruction techniques. The available image products include cylindrical and azimuthal projection scatterometer and SAR σ^o images with 1- and 3-day imaging intervals, and azimuthal projection scatterometer σ^o images with an 8-day imaging interval that have been further corrected for incidence and azimuth angle variation over the Greenland and Antarctic ice sheets. These σ^o image time series are compatibly-gridded with CETB and SETB T^B image time series to support a wide variety of geophysical applications.**

***Index Terms*—Soil Moisture Active Passive, scatterometry, synthetic aperture radar, radar backscatter, image reconstruction**

I. Introduction

Together, the NASA-funded MEaSUREs Calibrated Passive Microwave Daily *EASE-Grid 2.0* Brightness Temperature (CETB) Earth System Data Record [1], and the SMAP Radiometer Twice-Daily rSIR-Enhanced *EASE-Grid 2.0* Brightness Temperature (SETB) Data Set [2] provide an extensive multi-instrument, multi-decadal, time series of global enhanced-resolution microwave radiometer image products. The sequence of multi-frequency (Ka-band–L-band) instruments span from early in the satellite era to the present date, and include five Earth-observing satellite missions: (1) NASA's Nimbus-7 Scanning Multichannel Microwave Radiometer (SMMR, 1978-1987), (2) the Defense Meteorological Satellite Program (DMSP) Special Sensor Microwave/Imager (SSM/I, 1987-2021) and (3) Special Sensor Microwave Imager/Sounder (SSMIS, 2005-present) series, (4) NASA's Aqua Advanced Microwave Scanning Radiometer–Earth Observing System (AMSR-E, 2002-2011), and (5) NASA's Soil Moisture Active Passive (SMAP) microwave radiometer (2015-present). Earth-based, morning and evening images are generated using swath-based microwave brightness temperature (T^B) observations and image reconstruction techniques derived from irregular sampling deconvolution that are optimized for individual satellite missions [3], [4], [5], [6].

This paper describes new global enhanced-resolution SMAP scatterometer and synthetic aperture radar (SAR) image products generated by adapting previously developed image reconstruction techniques [7]. L-band (1.26 GHz) radar backscatter (σ^o) observations collected by the SMAP radar have been previously processed into two swath-based products: (1) low-resolution scatterometer-mode 'footprint' and 'slice' σ^o observations, and (2) high-resolution ground-processed SAR-mode σ^o observations [8]. We generate Earth-based, morning and evening images using the swath-based σ^o observations and the Scatterometer Image Reconstruction (SIR) algorithm [4], [7]. These consistently-processed, compatibility-gridded σ^o image time series are in important addition to the CETB and SETB archives that facilitate inter-comparison between satellite missions. The derived relationships can be exploited for geophysical studies over Earth's land surfaces, polar ice sheets, and global oceans.

II. NASA's Soil Moisture Active Passive Mission

NASA's SMAP mission was launched 31 January 2015 and began science operations 31 March 2015 [9]. The satellite flies at a 685 km altitude, 98.1° inclination, near-polar orbit with an 8-day exact repeat cycle and twice-daily Equator crossings at ~6 a.m. and 6 p.m. local-time-of-day.

The L-band instrument architecture integrates a novel hybrid radar [10] and a digital microwave radiometer [11] into a single measurement system that collects coincident σ^o and T^B observations. The radar and microwave radiometer share a deployable 6 m diameter parabolic mesh reflector that is offset from nadir and rotates on the nadir axis, providing a conically scanning antenna beam with a nominal surface incidence angle of ~40°. The antenna spin rate is 14.6 rpm, which, when coupled with the 6.86 km/s along-track ground velocity of the satellite, traces a helical antenna scan pattern on the Earth's surface with an along-track spacing of ~31 km between antenna rotations. The antenna scan pattern yields a 1000 km swath. Global coverage between latitudes of ~87°N and 87°S is achieved every 3 days. Unfortunately, the radar stopped transmitting 7 July 2015 as a result of an anomaly involving the high-power amplifier. The microwave radiometer was unaffected by the anomaly, and is currently operational.

The SMAP radar is a quad-polar rotating pencil-beam scatterometer capable of unfocused SAR imaging [10]. The scatterometer design is similar to the SeaWinds mission that was flown in tandem on NASA's Quick Scatterometer (QuikSCAT) satellite and JAXA's Advanced Earth Observing Satellite 2 (ADEOS-II) [**?**]. Prior to failure, the radar operated at a frequency of 1.26 GHz with a 1 MHz linear frequency modulated chirp. It collected σ^o observations at HH, VV, HV, and VH polarizations for nearly 100 days. In scatterometer-mode, onboard range-Doppler processing resolved the low-resolution full antenna footprint (29×36 km) into 12 narrower higher-resolution slices (5x30 km). High-resolution SAR-mode was achieved by ground processing the σ^o observations collected by the satellite over the outer ∼70% of the swath. The inner ∼30% of the swath was degraded and not used in the calculations. Antarctica was also excluded, with the exception of a limited number of σ^o observations collected over the Antarctic Peninsula during the first part of the operational period. The measurement accuracy is ∼1 dB for HH and VV, and ∼1.5 dB for HV and VH polarizations [9].

III. SMAP Enhanced-Resolution Scatterometer and Synthetic Aperture Radar Image Products

We generate SMAP enhanced-resolution scatterometer image products from SMAP Level-1B Radar Half-Orbit Time-Ordered Low-Resolution σ^o Data, Version 1, which are processed at the Jet Propulsion Laboratory (JPL) and archived and distributed by the NASA Alaska Satellite Facility (ASF) Distributed Active Archive Center (DAAC) [8]. This product provides time-ordered, parsed telemetry data collected by the SMAP radar during the 6 a.m. (descending) and 6 p.m. (ascending) half-orbit passes. It includes swath-based footprints and slices. Similarly, we generate SMAP SAR image products from SMAP Level-1C Radar Half-Orbit High-Resolution σ^o Data on 1 km Swath Grid, which are also processed at JPL and archived and distributed by the NASA ASF DAAC [8]. Ground processed σ^o observations are multi-looked into a 1 km square swath-based gridding, where the center line of the grid corresponds to the satellite's nadir track on the Earth's surface. We note that while the SAR σ^o observations have a higher effective resolution (∼1–3 km) than footprints (∼30 km) and slices (∼10 km), they are not collected nor calculated over the global oceans, most islands, and Antarctica.

The SIR algorithm was developed to reconstruct low-resolution swath-based σ^o observations into both conventionally gridded (GRD) and enhanced-resolution (SIR) Earth-based σ^o images [4]. The algorithm has been extensively applied to satellite scatterometer missions, such as the SeaWinds mission [7]. Conventionally gridded (GRD) images are generated by averaging all σ^o observations within a discrete imaging interval whose center locations fall within the bounds of a particular grid cell. GRD images provide low noise levels, but also low resolution. The SIR algorithm exploits the measurement response function (MRF) for each σ^o observation, which is a smeared version of the antenna footprint. Using the overlapping MRF's, the SIR algorithm reconstructs σ^o from the spatially filtered, low-resolution sampling provided by the swath-based σ^o observations. In effect, the SIR algorithm generates an MRF-deconvolved image. Combining multiple satellite orbital passes within a discrete imaging interval increases the sampling density, which improves the accuracy and resolution of the reconstruction [6]. Higher-resolution images generated using the SIR algorithm have higher noise levels. Thus, the differing GRD and SIR images provide a tradeoff between effective resolution and noise [4].

Low-resolution swath-based footprint and slice σ^o observations are processed into images using the SIR algorithm. We use the same algorithm that we used for the SeaWinds mission [7]. For simplicity, the antenna pattern is the squared (two-way versus one-way) antenna pattern used for the SMAP microwave radiometer processing. This simplified antenna pattern model ignores beam scan loss [12] that results from rotation of the antenna during the time of flight of the pulse between transmit and receive, which has only limited impact on the results. https://www.overleaf.com/project/61bcf6de062bfe2e3495f62c Slice GRD and SIR σ^o images are further corrected for incidence and azimuth angle variation across the satellite's wide (1000 km) swath using a simple second-order harmonic model [13]. The σ^o observations collected by the satellite are dependent on the surface incidence angle, especially over locations with steep topography, such as the Antarctic Peninsula and the Transantarctic Mountains. Additionally, locations with surface and subsurface roughness features, such as spatially coherent dune fields and sastrugi, exhibit azimuth angle dependence. Because the observation geometry varies between orbits, each satellite orbital pass results in a set of σ^o observations that have slightly different incidence and azimuth angles. When combining multiple satellite orbital passes these dependencies must be accounted for to avoid introducing artifacts into the images. There is a tradeoff between the imaging interval and the diversity in the incidence and azimuth angles. The observation geometry diversity is maximized at the 8-day exact repeat cycle of the satellite. Hence, slice SIR (3.125 km pixel) and GRD (25 km pixel) images are created using 8 days of data for each polarization, HH, VV, HV, and VH. The 8-day images overlay by 7 days so that an image is available for any contiguous 8-day period during the operational period.

We find that the spatial averaging inherent in footprint data results in limited sensitivity to incidence and azimuth angle, so geometric diversity is less of an issue for footprint measurements. To provide better temporal resolution for footprint measurements, 1-day and 3-day images GRD (25 km pixel) and SIR (3.125 km pixel) footprint images are created. The SAR images are created by gridding the SAR measurements into 3.125 km pixel grids on daily (1-day) and 3-day periods for HH, VV, and averaged HV-VH polarizations. As noted previously, the SAR data covers essentially only major land masses (minus Antarctica) and some islands. Except during the first few days when the radar operated in limited coverage test mode, no SAR data is available for Antarctica.

To exploit the orbit pass timing, two images per day are created for each of three regions defined in standard *EASE-Grid 2.0* projections. The global region (latitude within ±72°)a combines over the time period 6 a.m.–6 p.m. (the descending half-orbit pass) and 6 p.m.–6 a.m. (the ascending half-orbit

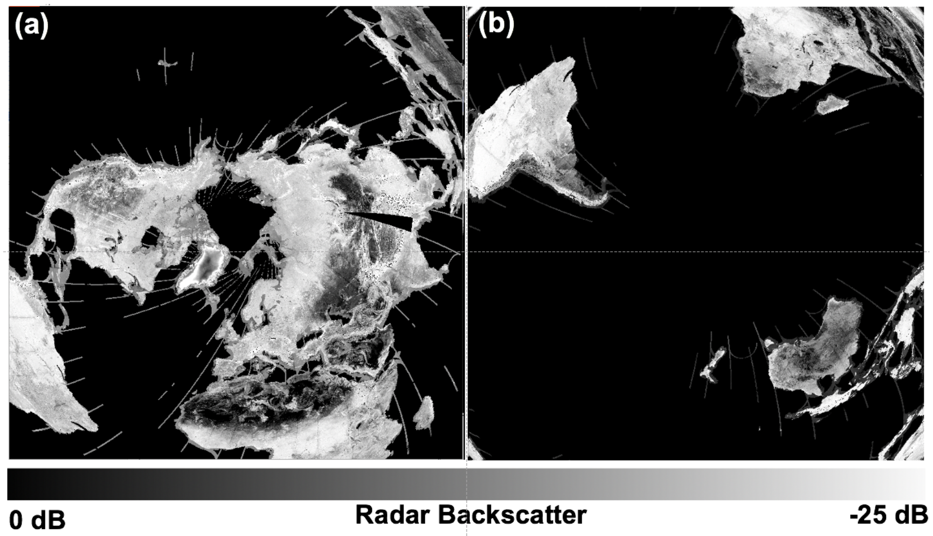

Fig. 1. Example SMAP radar polar stereographic morning images with data from 4-6 July 2015 made with SAR image data (clipped and shrunk for presentation here). (a) VV over the northern hemisphere. (b) HH over the southern hemisphere. The SAR data does not cover Antarctica.

pass) local-time-of-day. *EASE-Grids 2.0* Northern Hemisphere and Southern Hemisphere azimuthal images are generated 8 a.m.–4 p.m. (morning orbit passes) and 4 p.m.–8 a.m. (evening orbit passes)local-time-of-day. This minimizes fluctuations in observations at high latitudes due to changes in the physical temperature from local daily temperature cycling, and provides improved temporal resolution, permitting resolution of diurnal variations [5]. The image products covers the full operational time period of the SMAP radar, 13 April 2015–7 July 2015.

The effective resolution for each grid cell is dependent on the number of observations used in the algorithm and the measurement response function of the measurements used. The effective resolution is coarser than the grid cell spacing. The effective resolution of slice GRD σ^o images is $\sim$10 km, while slice SIR σ^o effective resolution is $\sim$6 km. Image reconstruction improves the effective resolution of GRD T^B images and slice GRD σ^o images by up to 60% [6]. The SAR image resolution is 3.125 km.

Some illustrative examples of the new SMAP radar image products are shown in Figs. 1-3. These compare the coverage and resolution of some of the products. While the SMAP SAR data provide finer resolution, they do not cover Antarctica. Scatterometer-mode data provides global coverage, but at much lower resolution. By applying reconstruction techniques the enhanced resolution products provide finer spatial resolution than conventional processing, which enables studies of smaller scale geophysical processes.

IV. Conclusion

Though limited in time, SMAP radar measurements provide an additional tool for studying geophysical processing. Our goal in producing these new twice-daily image products is to facilitate application of the data. It is our hope that providing SMAP radar on compatible grids to the existing CETB and SETB data set will facilitate its use in geophysical studies, particularly of the polar regions.

References

[1] M. J. Brodzik, D. G. Long, and M. A. Hardman, A. Paget, and R. Armstrong. "MEaSUREs Calibrated Enhanced-Resolution Passive Microwave Daily EASE-Grid 2.0 Brightness Temperature ESDR, Version 1." NASA National Snow and Ice Data Center DAAC, Boulder, CO USA, Tech. Rep., 2016.

[2] M. J. Brodzik, D. G. Long, and M. A. Hardman, "SMAP Radiometer Twice–Daily rSIR–Enhanced EASE-Grid 2.0 Brightness Temperatures, NASA National Snow and Ice Data Center Distributed Active Archive Center, Tech. Rep., 2021.

[3] D. G. Long and D. L. Daum, "Spatial resolution enhancement of SSM/I data," *IEEE Transactions on Geoscience and Remote Sensing*, vol. 36, no. 2, pp. 407–417, 1998.

[4] D. S. Early and D. G. Long, "Image reconstruction and enhanced resolution imaging from irregular samples," *IEEE Transactions on Geoscience and Remote Sensing*, vol. 39, no. 2, pp. 291–302, 2001.

[5] D. G. Long and M. J. Brodzik, "Optimum image formation for spaceborne microwave radiometer products," *IEEE Transactions Geoscience and Remote Sensing*, vol. 54, no. 5, pp. 2763–2779, 2016.

[6] D. G. Long, M. Brodzik, and M. Hardman, "Enhanced resolution SMAP brightness temperature image products," *IEEE Transactions on Geoscience and Remote Sensing*, vol. 57, no. 7, pp. 4151–4163, 2019

[7] D. G. Long, "Comparison of SeaWinds Backscatter Imaging Algorithms," *IEEE Journal of Selected Topics in Applied Earth Observations*, vol. 10, no. 3, pp. 2214–2231, 2017.

[8] R. West, "Soil Moisture Active and Passive Mission (SMAP) L1B S0, L1C S0 Algorithm Theoretical Basis Document (ATBD)," JPL, 27 Oct 2014.

[9] D. Entekhabi, S. Yueh, P. E. O'Neill, K. H. Kellog, A. Allen, R. Bindlish, *et al.*, "SMAP handbook–soil moisture active passive: Mapping soil moisture and freeze/thaw from space," Jet Propulsion Laboratory, Pasadena, CA, USA, Tech. Rep. JPL CL#14-2285, 2014.

[10] M. Spencer, S. Chan, and L.Veilleux, and K. Wheeler, "The Soil Moisture Active/Passive (SMAP) mission radar: A novel conically scanning SAR," *2009 IEEE Radar Conference,* pp. 1–4, 2009.

[11] J. Piepmeier, et al., "SMAP L-Band Microwave Radiometer: Instrument Design and First Year on Orbit," *IEEE Transactions on Geoscience and Remote Sensing,* vol. 55, no.4, pp. 1954–1966, 2017.

[12] F. Ulaby and D.G. Long, *Microwave Radar and Radiometric Remote Sensing*, ISBN: 978-0-472-11935-6, University of Michigan Press, Ann Arbor, Michigan, 2013.

[13] D.G. Long and M.R. Drinkwater, "Azimuth variation in microwave scatterometer and radiometer data over Antarctica," *I*EEE Transactions on Geoscience and Remote Sensing, vol. 38, no. 4, pp. 1857-1870, 2000.

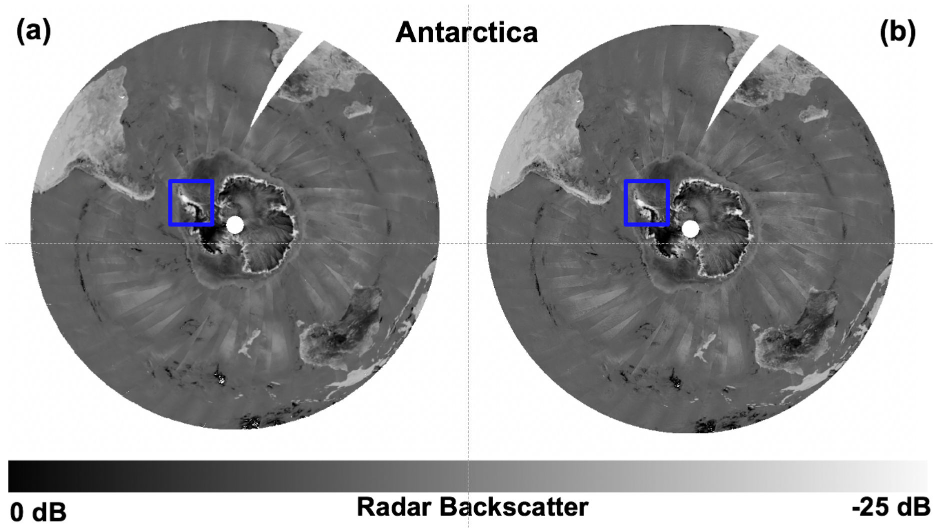

Fig. 2. SMAP radar morning HV-polarization image examples with data from 1-3 June 2015. (a) HV non-enhanced gridded scatterometer-mode. (b) SIR-enhanced resolution scatterometer mode. See Fig. 3 for zoom in of area indicated by blue box. Over the ocean and open water, azimuth direction and temporal variations in the wind-induced backscatter can produce 'herring bone' artifacts.

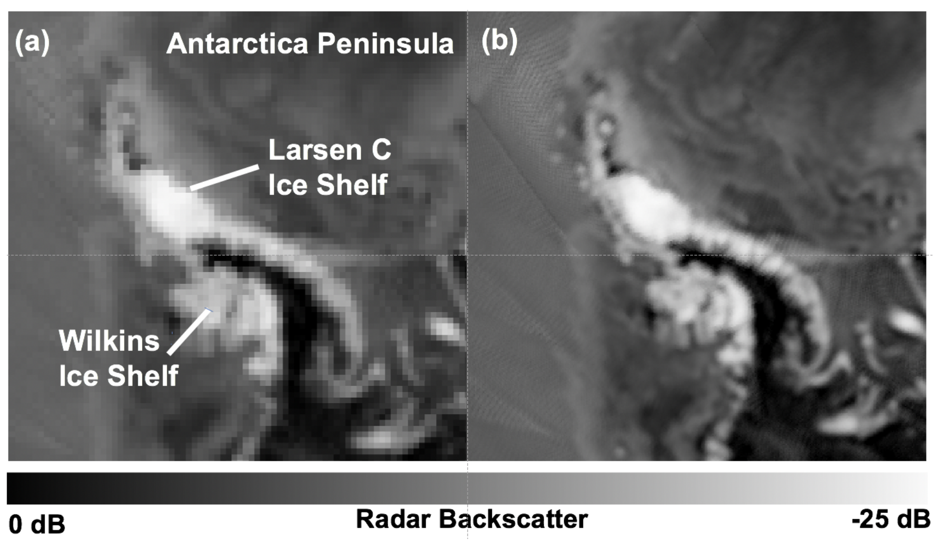

Fig. 3. Zoom-in of study regions indicated in Fig. 2. (a) HV non-enhanced gridded scatterometer-mode. (b) SIR-enhanced resolution scatterometer mode. Note the finer effective resolution of the SIR-enhanced image.